Journal of Alloys and Compounds, 765 (2018) 437-443

Correction of the shape effect on magnetic entropy change in ball milled Fe70Zr30 alloys

A.F. Manchón-Gordón, J.J. Ipus, L.M. Moreno-Ramírez, J.S. Blázquez*, C.F. Conde, V. Franco, A. Conde

Dpto. Física de la Materia Condensada, ICMSE-CSIC, Universidad de Sevilla, P.O. Box 1065, 41080 Sevilla, Spain
**The corresponding author e-mail:* jsebas@us.es

ABSTRACT: The field dependence of the magnetic entropy change (ΔS_M) after mechanical alloying of $Fe_{70}Zr_{30}$ composition starting from high purity powders is studied. Samples with different shapes and different crystalline fraction X were analyzed. Although, the results show that the proposed correction of the demagnetizing field has not a significant effect on $\Delta S_M(T)$ curves (~5 % underestimation), it is necessary in order to properly analyze the field dependence of this magnitude ($|\Delta S_M| = aH^n$). This correction allows recovering the theoretically predicted field dependence as well as a deeper analysis on multiphase systems. In fact, the biphasic character of the studied system changes the value of the field exponent n: it decreases below two above Curie temperature (T_C), and it increases at T_C. We show that assuming a non-interacting phase model, it is possible to obtain the value of the exponent n for the main phase from the intercept of n vs $X/\Delta S_M$.

KEYWORDS: magnetocaloric effect, mechanical alloying, amorphous alloys

1. INTRODUCTION

The magnetic refrigeration at temperatures close to room temperature, based on using the magnetocaloric effect (MCE), have received considerable attention in the research community due to its possibilities as a green and energy efficient technology [1-5]. The different magnetocaloric materials (i.e. those that show a significant MCE) can be

classified in terms of the character of the phase transition that these materials experience: a first order magnetic/magnetostructural phase transition (FOPT) or a second order magnetic transition (SOPT). The most significant compounds in the former category are $Gd_5(Si,Ge)_4$ [6], $La(Fe,Si)_{13}$ type alloys [7], MnAs [8] and NiMn-based Heusler alloys [9]. Although these materials are characterized by a larger MCE response at the transition temperature, thermal and magnetic hysteresis phenomena are present, which are detrimental for their use for commercial applications. In the second category, Gd has been the paradigmatic material for magnetic refrigeration around room temperature [10], with a negligible hysteresis. However, the main problem for this material is its high cost and its scarcity. In this second category, soft magnetic amorphous alloys are also present. Although the MCE in these systems is not really in competition with Gd or FOPT systems, they have an easily tunable Curie temperature with minor compositional changes and they present an extremely reduced magnetic hysteresis [11-14].

On the other hand, the field dependence of MCE for SOPT is well established [15] allowing useful predictions for the systems. It has been shown that several artefacts strongly affect this field dependence analysis as neglecting demagnetizing field and multiphase character of the samples [16, 17]. Calculating the demagnetizing field for non-ellipsoid samples is complicated. However, several approaches can be found in the literature to describe a set of spherical particles [18-20], which can describe a package of powder samples or nanocrystalline system were nanometer size crystals are embedded in a residual amorphous matrix.

The versatility of mechanical alloying (MA) technique and its ability to produce metastable phases make it to be widely used to produce supersaturated solid solutions and other metastable systems, including amorphous alloys [21]. This technique presents

various advantages (e.g. prevents the loss of volatile elements). However, powder samples prepared via MA present a non-negligible demagnetizing factor and the possibility of multiphase character (due to remnant impurities or contamination).

In this work, we have taken into account and studied several aspects inherent to powder samples on mechanically alloyed $Fe_{70}Zr_{30}$ composition, showing the importance of the demagnetizing factor for the correct magnetic characterization of the samples. In order to test the procedure followed to correct the demagnetizing field effect, samples with different external shapes were studied.

2. EXPERIMENTAL

Thirty grams of high purity (99.98%) elements powder mixture of nominal composition $Fe_{70}Zr_{30}$ were ball milled using steel balls and hardened steel vials in a Fritsch Pulverisette Vario 4 planetary mill. The ball to powder ratio was 10:1 and the ratio between the rotational speeds of the vials and the main disk was -2. Continuous milling steps of 0.5 h were performed in Ar atmosphere and after selected times, approximately 0.2 g of sample was extracted in a Saffron Omega glove box with oxygen and humidity levels below 2 ppm under Ar atmosphere.

The microstructure was studied by X-ray diffraction (XRD) using Cu-Kα radiation in a Bruker D8 I diffractometer. The local environment of Fe atoms was analyzed by Mössbauer spectrometry (MS) in transmission geometry at room temperature (RT) using a ^{57}Co(Rh) source. Values of the hyperfine parameters were obtained by fitting with NORMOS program [22] and the isomer shift (IS) was quoted relative to the Mössbauer spectrum of an α-Fe foil at RT.

Magnetic properties were measured using a Lakeshore 7407 Vibrating Sample Magnetometer (VSM) using a maximum applied field of $\mu_0 H$=1.5 T. Isothermal magnetization curves were measured from 100 to 390 K with increments of 10 K

(100< T<200 and 300< T<390) and 5 K (200< T<300). For the powders milled for 50 h, two types of sample shapes were prepared to obtain different demagnetizing factors. In the first case, the powder sample was pressed in silver capsules with a hydrostatic press of 2 tons to obtain disks of 4.5 mm diameter and ~0.3 mm thick (this method was also applied to obtain disk samples after 6.5, 8.5, 12.5, 16 and 30 h milling). In the second case, loose powder was packed in a silver capsule and, in order to prevent powder movement during measurements, a glue was added obtaining a roughly cylindrical shape that will be named in the following as irregular. The mass of the samples was measured in a Mettler Toledo XP 26 microbalance which provides a resolution of 0.001 mg.

Magnetic entropy change was calculated from isothermal magnetization curves using the Maxwell relation performed with the help of the Magnetocaloric Effect Analysis Program [23], available from LakeShore Cryotronics Inc. In all cases (disk and irregular samples), the magnetic field was applied perpendicular to the symmetry axis. From the analysis of the magnetic entropy change, we obtain the values of the exponent n, that describe its field dependence ($|\Delta S_M| = aH^n$).

3. RESULTS and DISCUSION

3.1. Microstructural characterization

Figure 1 shows, as an example, the evolution of RT Mössbauer spectra for samples obtained after 8.5, 16 and 50 h milling. Two ferromagnetic sites were used to fit the residual α-Fe(Zr) phase: a sextet with hyperfine field, HF=33 T (no Zr atoms in the neighborhood), and another with HF=30.5 T (one Zr atom in the neighborhood). A quadrupolar distribution was used to describe the amorphous phase. Moreover, a distribution of hyperfine fields from 0 to 30 T was used to show the contribution from

the interface region and richer Zr neighborhoods. The amorphous phase contribution continuously increases as milling time progresses. For the sample after 50 h milling, crystalline Fe sites at 33T and 30.5 T were not detected.

XRD patterns of samples obtained after different milling times are shown in figure 2. The amorphous phase of the as-milled samples is evidenced after 6 h milling by the appearance of a wide amorphous halo. The bcc Fe maxima get broader as milling time increases due to the reduction of the crystal size of this phase. Peaks attributed to the hcp Zr phase are only present for short milling times (t<6 h), showing that this phase becomes imperceptible as the Zr atoms become dissolved in the Fe amorphous matrix. In the case of the sample after 50 h milling, crystalline phase is not detected. However, a detailed analysis combining XRD and Mössbauer spectroscopy has shown the presence of a small amount of bcc-$Fe_{95}Zr_5$ crystalline phase even after 50 h milling [24].

3.2 Magnetic characterization

Figure 3 shows, as an example, the temperature dependent magnetization at different applied magnetic fields displayed for samples after 8.5, 16 and 50 h of milling. For all applied fields, a decrease of the magnetization is observed due to the Curie transition of the amorphous phase. Magnetization does not fall to zero because of the presence of the residual ferromagnetic α-Fe type phase, which has a higher Curie temperature than the amorphous one. As milling time increases, this fall is enhanced due to the increase of the amorphous fraction, in agreement with the evolution of the XRD patterns.

In order to measure the Curie temperature of the different samples, low field magnetization ($\mu_0 H$=0.001 T) curves were analyzed. The inflexion point detected allows us to estimate T_C. However, the broad maximum in dM/dT is consistent with a distribution of Curie temperatures due to the presence of composition/microstructural

inhomogeneities induced during the milling process [25]. The increase of T_C (table 1) as milling time increases is in agreement with a Fe enrichment in the amorphous phase.

3.3 Sample shape effect

Demagnetizing field H_D is a factor to take into account when characterizing magnetic properties of powder samples. In these cases, the magnetic field H inside the sample can be calculated as:

$$H = H_{app} - N_D M \quad (1)$$

where H_{app} is the applied magnetic field, M is the magnetization and N_D is the demagnetizing factor. A non-negligible N_D affects the measurements of the magnetic susceptibility as:

$$\chi^{-1} = \frac{H}{M} = \frac{H_{app} - N_D M}{M} = \chi_a^{-1} - N_D \quad (2)$$

where χ is the magnetic susceptibility of the material and χ_a is the measured (apparent) susceptibility of the sample. In the case of materials with large magnetic susceptibility ($\chi^{-1} \ll N_D$), N_D can be determined as the inverse of the apparent susceptibility. To observe this situation, two conditions must be fulfilled: 1) For a constant and low H_{app}, M should be independent of the temperature in a certain range below the Curie temperature; 2) For a constant temperature, M should be proportional to the applied magnetic field for low enough values of H_{app}. Figure 4 shows M vs H_{app} for both samples with disk and irregular form of $Fe_{70}Zr_{30}$ alloys after 50 h of milling. At low temperatures (T<180 K) a linearity can be observed between M and H_{app} at low fields, which can be considered as a limit found when T and H_{app} are low enough. This tendency can be used to determine the demagnetizing factor, being N_D=0.109±0.003

and N_D=0.247±0.002 for the disk and the irregular samples, respectively. Bleaney and Hull [19] proposed an approximation to obtain the demagnetizing factor in a package of powder particles:

$$N_D^{total} = N_D^{particle} + f\left(N_D^{pack} - N_D^{particle}\right) \quad (3)$$

where N_D^{total}, $N_D^{particle}$ and N_D^{pack} are the demagnetizing factor of the whole sample, the powder particle and the pack, respectively, and f is the packing fraction. Equation 3, in the limit of full density, reduces to the demagnetizing factor of the geometry of the pack. For loosely packed powder particles (f~0), N_D^{total} reduces to that of the particles.

Figure 5 shows the magnetic entropy change for a maximum field change of 1 T as a function of temperature, obtained with and without correcting the demagnetizing field for the two samples after 50 h milling. Neglecting the demagnetizing field slightly affects the magnetic entropy change [26]. Error bars of the experimental data would be mainly due to mass measurement (error below 0.1 %), whereas magnetization measurements have a much smaller error for the samples studied here (~0.5 emu for a sample of ~10 mg). In any case, the small difference shown in ΔS_M with and without correction is larger than the experimental errors. However, the most important effect is observed in the field dependence of the MCE response [17, 27]. Unlike previous papers, where the demagnetizing factor of a sphere (N_D=1/3) was assumed, in the present paper N_D was directly estimated for each sample from the behavior of apparent magnetic susceptibility at low fields and at low temperatures. This field dependence, assuming a zero starting field, can be written as [28]:

$$|\Delta S_M(H,T)| = a(T)H^{n(H,T)} \quad (4)$$

For single phase systems with a second-order transition it has been demonstrated that exponent n is field independent in three regions: well below the Curie temperature

(n=1), well above the transition (n=2) and at Curie temperature, where n is related with the critical exponents [28]. The temperature dependence of exponent n is shown in figure 6 for $\mu_0 H$=1 T with and without correcting the demagnetizing field for the samples after 50 h milling. After correcting the demagnetizing field below T_C, the value of $n \leq 1$ qualitatively agrees with the expected one for materials presenting a ferromagnetic behavior. For $T > T_C$ there is no effect of demagnetizing field, as expected.

Recently, Bjork and Bahl [20] performed some calculations to obtain effective demagnetizing factors for aggregates of spherical particles and found that N_D increases as permeability decreases. Using an iterative process, we have corrected our $M(H)$ curves considering a non-constant N_D, but the differences are negligible (less than 1% in n at T_C).

3.4. Effect of impurities

For $T > T_C$ an increase of n is observed, but the expected value (n=2) for paramagnetic materials is not reached. This has been previously observed for other kind of materials and was ascribed to the biphasic character of the samples [29]. In our case, this is in agreement with the crystalline remnant contribution observed from Mössbauer data. Therefore, n shows a value between one, corresponding to ferromagnetic α-Fe(Zr) impurities, and two, corresponding to the paramagnetic amorphous phase, depending on the amorphous phase fraction of the sample. To show this dependency, different partially amorphous samples have been studied. Different samples milled for 6.5, 8.5, 12.5, 16 and 30 h were prepared with a disk shape form and their demagnetizing factor N_D were determined as described in section 3.1. Values are shown in table 1.

Figure 7 shows the magnetic entropy change for disk samples from powder milled 8.5, 16 and 50 h, for a maximum field change of 1 T as a function of temperature with and

without correcting the demagnetizing field. As milling time increases, an increase of $|\Delta S_M|$ is observed due to the increase of the amorphous fraction, which is the responsible of the studied magnetic transition [30]. $|\Delta S_M|$ curve becomes broad and reaches a maximum value of about -0.45 $Jkg^{-1}K^{-1}$ at 233 K for the sample after 50 h of milling. This value of $|\Delta S_M|$ is similar to those reported in the literature for samples with the same compositions prepared by ball milling [31]. However, $|\Delta S_M|$ is smaller than the values observed for amorphous ribbon samples prepared by rapid quenching techniques with similar compositions (see table 2). In the case of the rapidly quenched samples, it is worth noting that T_C is strongly dependent on Fe content. The $\Delta S_M(T)$ curves for rapidly quenched amorphous alloys are also sharper than those of samples prepared by milling, indicating a stronger inhomogeneity in the latter type of samples [17].

Figure 8 shows the temperature dependence of the exponent n for μ_0H=1 T with and without correcting the demagnetizing field for the samples milled 8.5, 16 and 50 h. For temperatures well below T_C, n values corrected for the effect of demagnetizing factor tend to 1, as expected. An increase of n at $T>T_C$ is clearly observed as milling time increases, i.e. as amorphous fraction increases.

The behavior of n at T_C and well above T_C can be explained considering the biphasic character of our samples. Assuming non-interacting phases, the total magnetic entropy change of a biphasic system can be estimated as [16]:

$$\Delta S_M = a_{imp} X H^{n_{imp}} + a_{main}(1-X)H^{n_{main}} \quad (5)$$

where the indexes *main* and *imp* correspond to the main phase (amorphous) and the impurity phase (bcc-crystals), respectively and X is the fraction of the impurity phase. In our case, for ferromagnetic impurities with a Curie temperature higher than that of the phase of interest (amorphous phase), n can be obtained as [29]:

$$n = \frac{a_{imp} H}{\Delta S_M} X\,(1 - n_{main}) + n_{main} \quad (6)$$

Therefore, from the intercept of n vs. $X/\Delta S_M$ it is possible to obtain a value of n_{main}. This analysis was applied in two situations: at T_C and at temperatures well above T_C, for which exponent n has a local maximum (T=315 K for samples milled for 6.5 and 8.5, T=325 K for samples milled for 12.5, 16 and 30 h and T=355 K for sample milled for 50 h).

Using data at T_C for the different studied samples (figure 9), an exponent n_{main}=0.845±0.005 is extrapolated for a pure amorphous phase. Some examples of the different n_{main} results achieved at T_C on rapid quenched and ball-milled transition metal based alloys are summarized in table 3. Value of n_{main} at T_C obtained in this work are generally higher than those found from rapidly quenched alloys [17]. This effect has been found in mechanically alloyed samples and ascribed to a distribution of Curie temperatures [17].

When applying equation 6 to a temperature well above T_C, where the plateau of n is reached, we also observed a linear trend for n that should reach 2 for X=0. Moreover, the intersection of both straight lines should be at n =1. These two features are observed with an error below 5% in figure 9. The observed deviations could be ascribed to neglecting the overlapping between the two transitions (amorphous and crystalline phases) and the presence of magnetic interactions between phases which are not considered in our model.

4. CONCLUSIONS

In this work, partially amorphous $Fe_{70}Zr_{30}$ alloys were prepared via mechanical alloying. Microstructure and Fe environments results show the increase of amorphous contribution with milling time. The use of low field and low temperature susceptibility

data to correct the demagnetizing field successfully yields results independent of the shape of the sample. Although this correction yields small differences in $\Delta S_M(T)$ curves, it is needed to appropriately account for the field dependence of this magnitude. The presence of ferromagnetic impurities has two effects: 1) It decreases the field exponent n in ΔS_M values above T_C with a tendency to n=2 for X=0, as theory predicts; and 2) it increases the exponent n values at T_C. The predicted linear behavior for the exponent n as a function of the ratio between the fraction of the crystalline phase and the magnetic entropy change is experimentally observed in the two studied regions (at T_C and well above T_C). As an evidence of internal consistency of the proposed model, the intersection of the two extrapolated lines is found close to n =1. The estimated value of n at T_C for a pure amorphous phase is higher than the expected values for amorphous alloys, which could be due to compositional inhomogeneity.

Acknowledgements

This work was supported by the Spanish MINECO and EU FEDER (Project MAT 2013-45165-P), AEI/FEDER-UE (Project MAT-2016-77265-R) and the PAI of the Regional Government of Andalucía. A.F. Manchón-Gordón acknowledges a VPPI-US fellowship from the University of Sevilla. L.M Moreno-Ramírez acknowledges a FPU fellowship from the Spanish MECD.

References

[1] Gschneidner KA, Pecharsky VK. Magnetocaloric materials. Annual Review of Materials Science 2000;30:387-429.
[2] Bruck E, Tegus O, Thanh DTC, Buschow KHJ. Magnetocaloric refrigeration near room temperature. Journal of Magnetism and Magnetic Materials 2007;310:2793-9.

[3] Gutfleisch O, Willard MA, Bruck E, Chen CH, Sankar SG, Liu JP. Magnetic Materials and Devices for the 21st Century: Stronger, Lighter, and More Energy Efficient. Advanced Materials 2011;23:821-42.
[4] Franco V, Blazquez JS, Ingale B, Conde A. The Magnetocaloric Effect and Magnetic Refrigeration Near Room Temperature: Materials and Models. Annual Review of Materials Research2012. p. 305-42.
[5] Franco V, Blazquez JS, Ipus JJ, Law JY, Moreno-Ramírez LM, Conde A. Magnetocaloric effect: from materials research to refrigeration devices. Progress in Materials Science 2018;93:112-232.
[6] Pecharsky AO, Gschneidner DA, Pecharsky VK, Schindler CE. The room temperature metastable/stable phase relationships in the pseudo-binary Gd5Si4-Gd5Ge4 system. Journal of Alloys and Compounds 2002;338:126-35.
[7] Hu FX, Shen BG, Sun JR, Cheng ZH, Rao GH, Zhang XX. Influence of negative lattice expansion and metamagnetic transition on magnetic entropy change in the compound LaFe11.4Si1.6. Applied Physics Letters 2001;78:3675-7.
[8] Tegus O, Bruck E, Buschow KHJ, de Boer FR. Transition-metal-based magnetic refrigerants for room-temperature applications. Nature 2002;415:150-2.
[9] Planes A, Manosa L, Moya X, Krenke T, Acet M, Wassermann EF. Magnetocaloric effect in Heusler shape-memory alloys. Journal of Magnetism and Magnetic Materials 2007;310:2767-9.
[10] Dan'kov SY, Tishin AM, Pecharsky VK, Gschneidner KA. Magnetic phase transitions and the magnetothermal properties of gadolinium. Physical Review B 1998;57:3478-90.
[11] Skorvanek I, Kovac J. Magnetocaloric behaviour in amorphous and nanocrystalline FeNbB soft magnetic alloys. Czechoslovak Journal of Physics 2004;54:D189-D92.
[12] Franco V, Blazquez JS, Conde CF, Conde A. A Finemet-type alloy as a low-cost candidate for high-temperature magnetic refrigeration. Applied Physics Letters 2006;88.
[13] Johnson F, Shull RD. Amorphous-FeCoCrZrB ferromagnets for use as high-temperature magnetic refrigerants. Journal of Applied Physics 2006;99.
[14] Wang DH, Peng K, Gu BX, Han ZD, Tang SL, Qin W, et al. Influence of annealing on the magnetic entropy changes in Fe81.6Mo4Zr3.3Nb3.3B6.8Cu1 amorphous ribbons. Journal of Alloys and Compounds 2003;358:312-5.
[15] Franco V, Conde A. Scaling laws for the magnetocaloric effect in second order phase transitions: From physics to applications for the characterization of materials. International Journal of Refrigeration-Revue Internationale Du Froid 2010;33:465-73.
[16] Blázquez JS, Ipus JJ, Moreno-Ramírez LM, Borrego JM, Lozano-Pérez S, Franco V, et al. Analysis of the Magnetocaloric Effect in Powder Samples Obtained by Ball Milling. Metallurgical and materials transactions E 2015;2:131-8.
[17] Moreno-Ramirez LM, Ipus JJ, Franco V, Blazquez JS, Conde A. Analysis of magnetocaloric effect of ball milled amorphous alloys: Demagnetizing factor and Curie temperature distribution. Journal of Alloys and Compounds 2015;622:606-9.
[18] Lefloch M, Mattei JL, Laurent P, Minot O, Konn AM. A PHYSICAL MODEL FOR HETEROGENEOUS MAGNETIC-MATERIALS. Journal of Magnetism and Magnetic Materials 1995;140:2191-2.
[19] Bleaney B, Hull RA. The effective susceptibility of a paramagnetic powder. Proceedings of the Royal Society of London Series A Mathematical and Physical Sciences 1941;178:86.
[20] Bjørk R, Bahl CRH. Demagnetization factor for a powder of randomly packed spherical particles. Applied Physics Letters 2013;103:102403.
[21] Suryanarayana C. Mechanical alloying and milling. Progress in Materials Science 2001;46:1-184.
[22] Brand RA, Lauer J, Herlach DM. THE EVALUATION OF HYPERFINE FIELD DISTRIBUTIONS IN OVERLAPPING AND ASYMMETRIC MOSSBAUER-SPECTRA: A STUDY OF THE AMORPHOUS ALLOY PD77.5-XCU6SI16.5FEX. Journal of Physics F-Metal Physics 1983;13:675-83.
[23] http://www.lakeshore.com/products/Vibrating-Sample-Magnetometer/Pages/MCE.aspx

[24] Manchon-Gordon AF, Ipus JJ, Blazquez JS, Conde CF, Conde A. Evolution of Fe environments and phase composition during mechanical amorphization of Fe70Zr30 and Fe70Nb30 alloys. Journal of Non-Crystalline Solids 2018.
[25] Alvarez-Alonso P, Llamazares JLS, Sanchez-Valdes CF, Cuello GJ, Franco V, Gorria P, et al. On the broadening of the magnetic entropy change due to Curie temperature distribution. Journal of Applied Physics 2014;115.
[26] Caballero-Flores R, Franco V, Conde A, Kiss LF. Influence of the demagnetizing field on the determination of the magnetocaloric effect from magnetization curves. Journal of Applied Physics 2009;105.
[27] Romero-Muniz C, Ipus JJ, Blazquez JS, Franco V, Conde A. Influence of the demagnetizing factor on the magnetocaloric effect: Critical scaling and numerical simulations. Applied Physics Letters 2014;104.
[28] Franco V, Blazquez JS, Conde A. Field dependence of the magnetocaloric effect in materials with a second order phase transition: A master curve for the magnetic entropy change. Applied Physics Letters 2006;89:222512.
[29] Blazquez JS, Moreno-Ramirez LM, Ipus JJ, Kiss LF, Kaptas D, Kemeny T, et al. Effect of alpha-Fe impurities on the field dependence of magnetocaloric response in LaFe11.5Si1.5. Journal of Alloys and Compounds 2015;646:101-5.
[30] Jones NJ, Ucar H, Ipus JJ, McHenry ME, Laughlin DE. The effect of distributed exchange parameters on magnetocaloric refrigeration capacity in amorphous and nanocomposite materials. Journal of Applied Physics 2012;111.
[31] Blazquez JS, Franco V, Conde A. Enhancement of the magnetic refrigerant capacity in partially amorphous Fe70Zr30 powders obtained by mechanical alloying. Intermetallics 2012;26:52-6.
[32] Kim KS, Kim YS, Zidanic J, Min SG, Yu SC. Magnetocaloric effect in as-quenched and annealed Fe91-xYxZr9 (x=0.5, 10) alloys. Physica Status Solidi a-Applications and Materials Science 2007;204:4096-9.
[33] Thanh TD, Yu Y, Thanh PT, Yen NH, Dan NH, Phan TL, et al. Magnetic properties and magnetocaloric effect in Fe90-xNixZr10 alloy ribbons. Journal of Applied Physics 2013;113.
[34] Mishra D, Gurram M, Reddy A, Perumal A, Saravanan P, Srinivasan A. Enhanced soft magnetic properties and magnetocaloric effect in B substituted amorphous Fe-Zr alloy ribbons. Materials Science and Engineering B-Advanced Functional Solid-State Materials 2010;175:253-60.
[35] Thanh TD, Yen NH, Duc NH, Phan TL, Dan NH, Yu SC. Large Magnetocaloric Effect Around Room Temperature in Amorphous Fe-Gd-Zr Alloy Ribbon with Short-Range Interactions. Journal of Electronic Materials 2016;45:2608-14.
[36] Franco V, Blazquez JS, Millan M, Borrego JM, Conde CF, Conde A. The magnetocaloric effect in soft magnetic amorphous alloys. Journal of Applied Physics 2007;101:1-3.
[37] Franco V, Blazquez JS, Conde A. The influence of Co addition on the magnetocaloric effect of Nanoperm-type amorphous alloys. Journal of Applied Physics 2006;100:064307.
[38] Moreno-Ramirez LM, Blazquez JS, Franco V, Conde A, Marsilius M, Budinsky V, et al. Magnetocaloric response of amorphous and nanocrystalline Cr-containing Vitroperm-type alloys. Journal of Magnetism and Magnetic Materials 2016;409:56-61.
[39] Ipus JJ, Moreno-Ramirez LM, Blazquez JS, Franco V, Conde A. A procedure to extract the magnetocaloric parameters of the single phases from experimental data of a multiphase system. Applied Physics Letters 2014;105:172405.

FIGURES

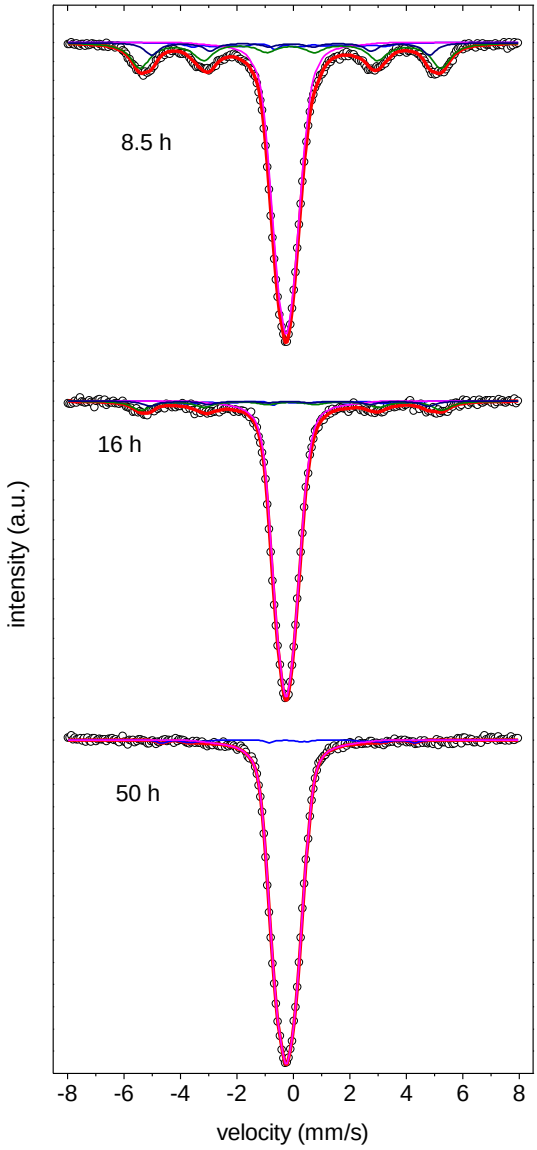

Figure 1. Experimental Mössbauer spectra (symbols) and model fitting (lines) for samples milled during 8.5, 16 and 50 h.

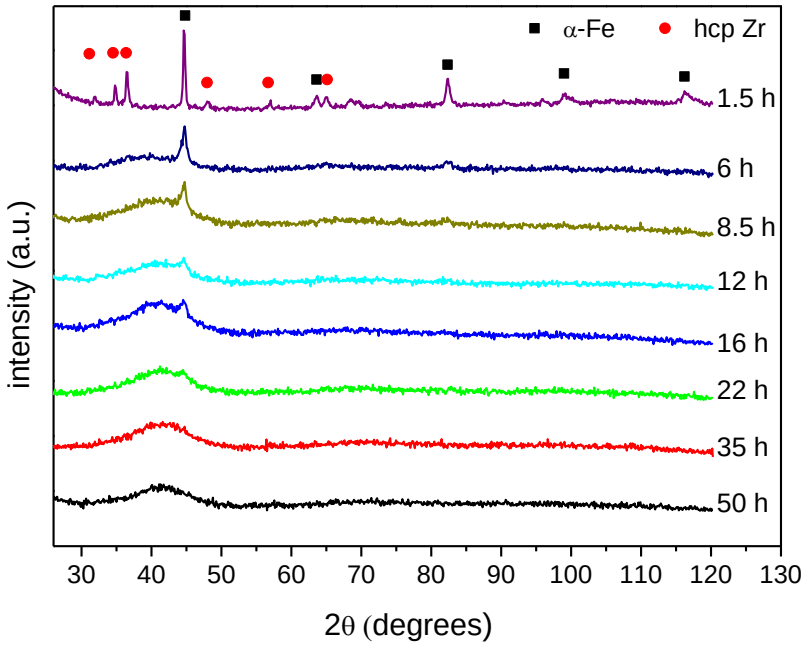

Figure 2. XRD patterns of the mechanically alloyed $Fe_{70}Zr_{30}$ powders for different milling times. Miller indexes from left to right: (α-Fe phase) (110), (200), (211), (220), (310); (hcp Zr) (100), (002), (101), (102), (110), (200).

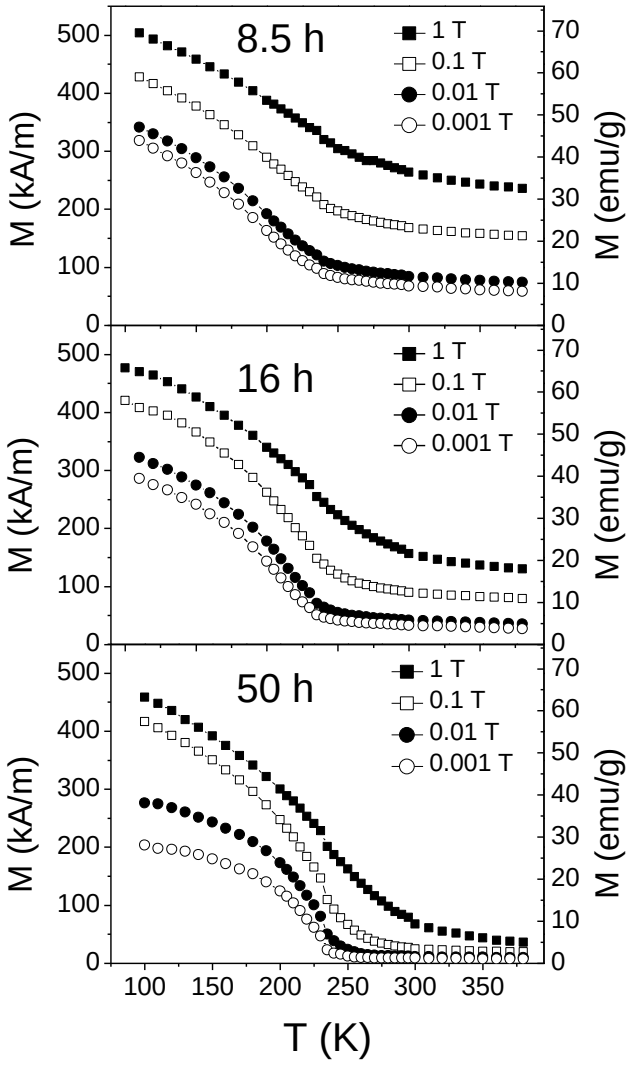

Figure 3. Magnetization at various constant applied field values as a function of temperature for three different samples.

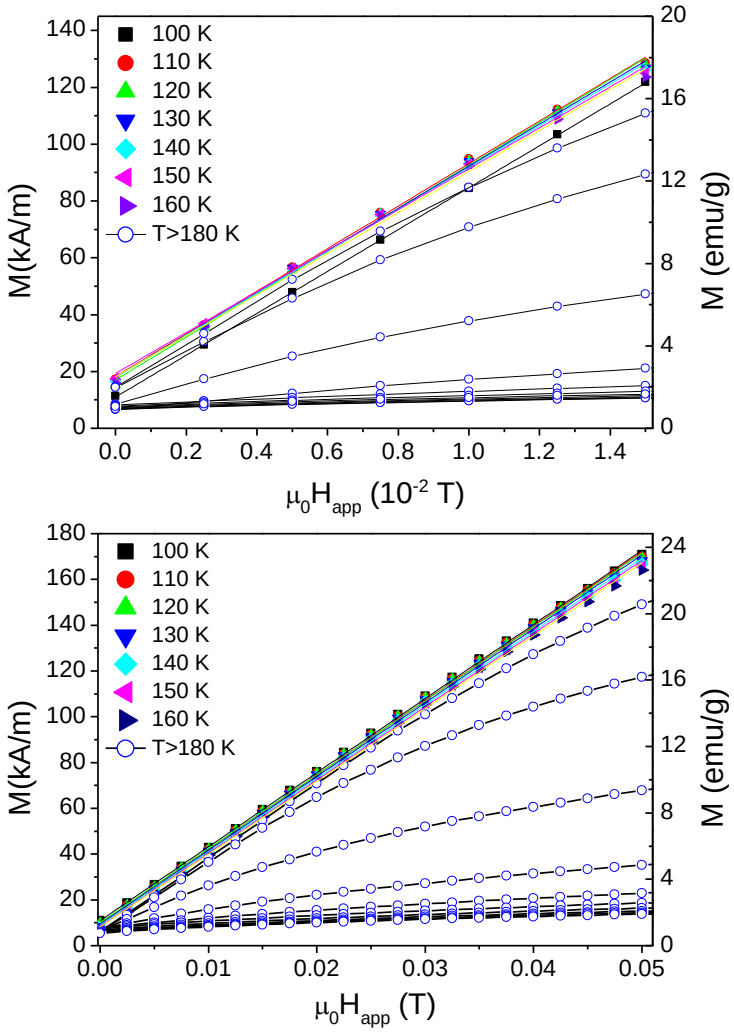

Figure 4. Isothermal magnetization curves for samples milled 50 h with disk form (above) and irregular form (below). Change from emu/g to A/m has been done assuming a density of 7205 kg/m^3.

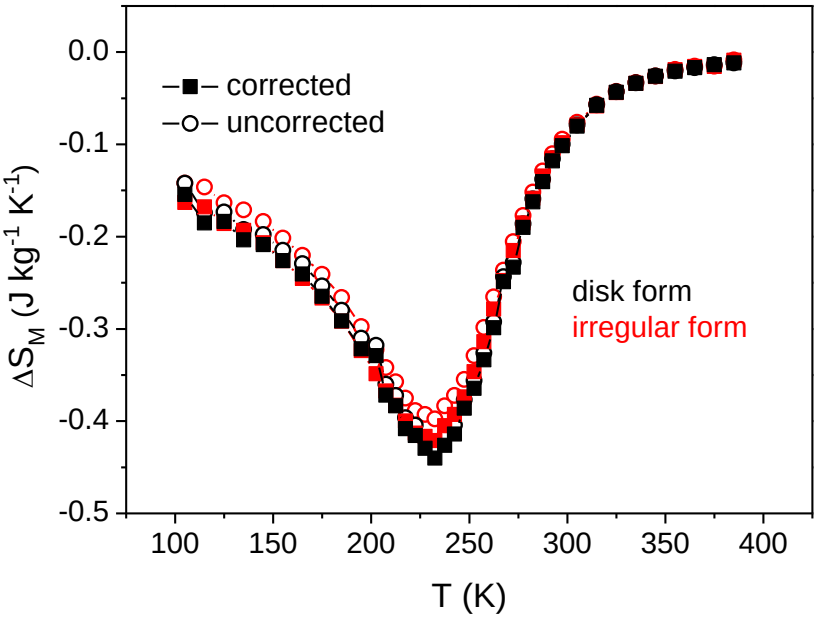

Figure 5. Magnetic entropy change at $\mu_0\Delta H$=1 T with (solid squares) and without (hollow circles) correcting the demagnetizing field for the two samples prepared using powders milled for 50 h.

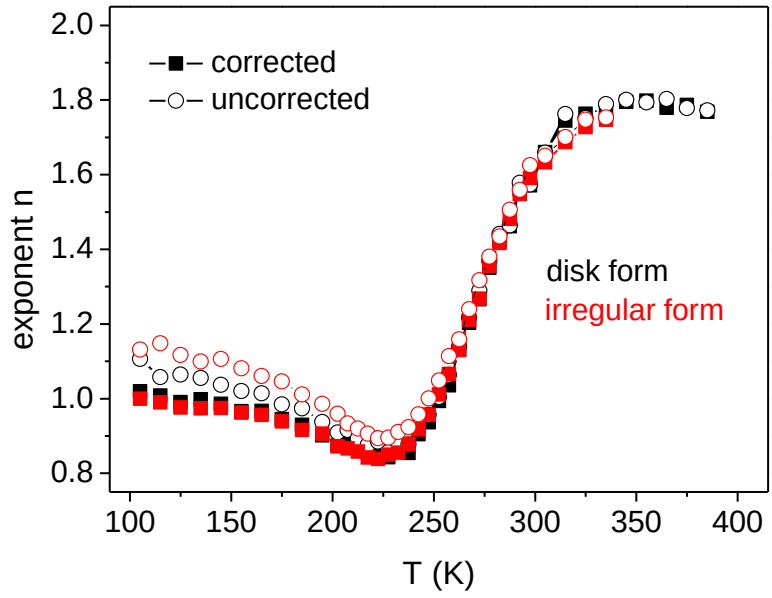

Figure 6. Temperature dependence of the n exponent characterizing the field dependence of ΔS_M with (solid squares) and without (hollow circles) correcting the demagnetizing field for the two samples prepared using powders milled for 50 h.

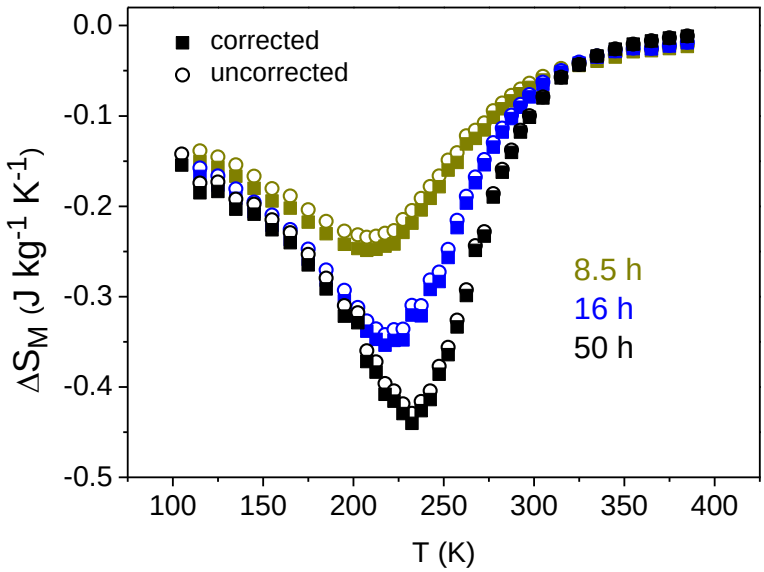

Figure 7. Magnetic entropy change at $\mu_0\Delta H$=1 T with (solid squares) and without (hollow circles) correcting the demagnetizing field for disk samples with different amorphous fractions.

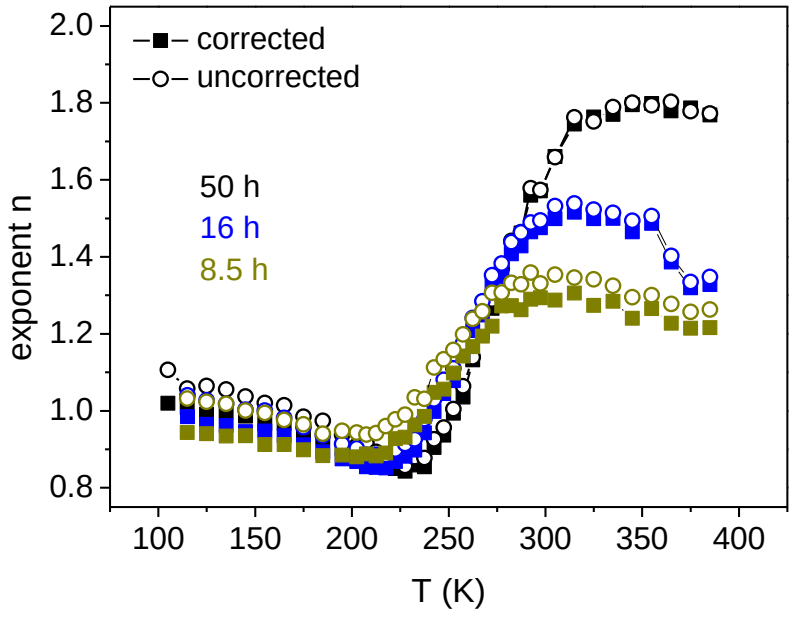

Figure 8. Temperature dependence of the n exponent characterizing the field dependence of ΔS_M with (solid squares) and without (hollow circles) correcting the demagnetizing field for disk samples with different amorphous fractions.

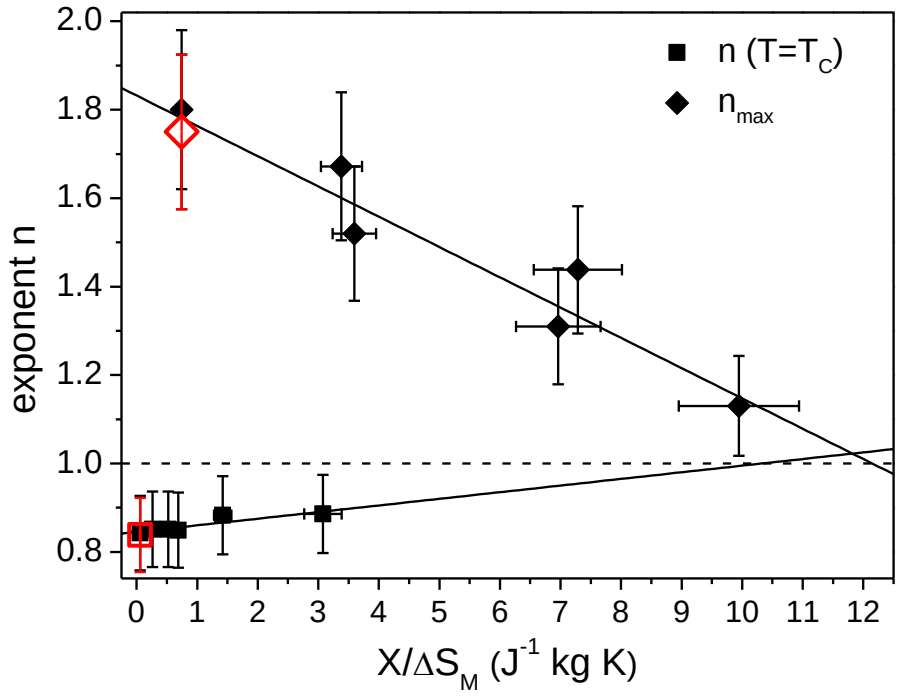

Figure 9. Exponent n vs $X/\Delta S_M$ at T=T_C (diamond) and at temperatures well above T_C, which one exponent n is maximum (square). Hollow symbols correspond to the values obtained for the sample with irregular form. The solid lines correspond to the linear fitting using Eq. (6).

Table 1. Curie temperatures (from inflexion point of M(T)) and demagnetizing factor of the disk samples from powder after different times of milling.

Time of milling (h)	T_C **(K)**	N_D
6.5	195	0.26±0.02
8.5	200	0.172±0.005
12.5	200	0.121±0.008
16	210	0.120±0.002
30	210	0.112±0.005
50	230	0.109±0.003

Table 2. Experimental values of $|\Delta S_M|$ for FeZr based alloys.

Composition	**Technique**	T_C **(K)**	$\mu_0 \Delta H$ **(T)**	$\|\Delta S_M\|$ **(Jkg^{-1}K^{-1})**	**Reference**
$Fe_{70}Zr_{30}$	Mechanical alloying	230	1	0.45	This work
$Fe_{70}Zr_{30}$	Mechanical alloying	244	1.5	~0.4	[31]
$Fe_{91}Zr_{9}$	Rapid quenching	233	1.5	1.22	[32]
$Fe_{90}Zr_{10}$	Rapid quenching	245	1	0.87	[33]
$Fe_{89}Zr_{11}$	Rapid quenching	263	1.8	1.3	[34]
$Fe_{88}Gd_2Zr_{10}$	Rapid quenching	285	1.5	1.4	[35]

Table 3. Summary of selected works on MCE where n_{main} has been calculated for transition metal-based amorphous alloys.

Composition	Technique	n_{main} at T_C	Reference
$Fe_{29}Co_{40}B_9C_2Si_3Al_5Ga_2P_{10}$ $Fe_{59}Co_{14}B_6C_4Si_3Al_5Ga_2P_{10}$	Rapid quenching	~0.71	[36]
$Fe_{83}Zr_6B_{10}Cu_1$	Rapid quenching	~0.74	[37]
$Fe_{72}Cr_2Cu_1Nb_3Si_{15.5}B_{6.5}$	Rapid quenching	~0.8	[38]
$Fe_{75}Nb_{10}B_{15}$	Mechanical alloying	0.757±0.012	[39]
$Co_{62}Nb_6Zr_2B_{30}$	Mechanical alloying	0.89	[17]
$Fe_{70}Zr_{30}$	Mechanical alloying	0.845±0.005	This work